



Regular article

Suppressed martensitic transformation under biaxial loading in low stacking fault energy metastable austenitic steels

E. Polatidis^a, W.-N. Hsu^{a,b}, M. Šmíd^a, T. Panzner^c, S. Chakrabarty^d, P. Pant^d, H. Van Swygenhoven^{a,b,*}

^a Photons for Engineering and Manufacturing Group, Swiss Light Source, Paul Scherrer Institute, Villigen-PSI 5232, Switzerland

^b Neutrons and X-rays for Mechanics of Materials, IMX, Ecole Polytechnique Fédérale de Lausanne, CH-1012 Lausanne, Switzerland

^c Laboratory for Neutron Scattering, NUM, Paul Scherrer Institute, Villigen PSI 5232, Switzerland

^d Department of Metallurgical Engineering and Materials Science, IIT Bombay, Mumbai 400076, India

ARTICLE INFO

Article history:

Received 13 October 2017

Received in revised form 19 December 2017

Accepted 23 December 2017

Available online 4 January 2018

Keywords:

Metastable stainless steel

Martensite

TRIP

Stacking fault

Partial dislocations

ABSTRACT

The effect of uniaxial/biaxial loading on the martensitic transformation of a low stacking fault energy, metastable austenitic stainless steel was studied by in-situ neutron diffraction on cruciform-shaped/dogbone samples. Uniaxial loading favors the martensitic transformation following the sequence $\gamma \rightarrow \varepsilon \rightarrow \alpha'$, where at low strains ε -martensite is the precursor of α' . During equibiaxial-loading, the evolving texture suppresses the formation of ε -martensite and considerably less α' -martensite is observed at high strains. The results are discussed with respect to the deformation textures, the loading direction and the mechanism of the ε -martensite transformation. © 2018 Acta Materialia Inc. Published by Elsevier Ltd. This is an open access article under the CC BY-NC-ND license (<http://creativecommons.org/licenses/by-nc-nd/4.0/>).

In metastable austenitic stainless steels martensite forms upon deformation, the so-called transformation induced plasticity or TRIP effect, and this transformation is responsible for a good combination of strength and ductility that these materials exhibit. Two types of martensite can be formed during deformation: the hexagonal-closed-packed (hcp) ε -phase and the body-centered-cubic/tetragonal (bcc or bct) α' -phase. For some steels, it has been reported that ε -martensite is a precursor of α' -martensite as it forms at early stages of plastic deformation and that α' forms at later stages of deformation in expense of ε -martensite [1–4]. For other steels the direct formation of $\gamma \rightarrow \alpha'$ has been reported [5]. Generally it is believed that the prevalence of $\gamma \rightarrow \varepsilon \rightarrow \alpha'$ or $\gamma \rightarrow \alpha'$ depends on the stacking-fault-energy (SFE) of the austenitic phase: for low SFE steels ($<20 \text{ mJm}^{-2}$) the sequence $\gamma \rightarrow \varepsilon \rightarrow \alpha'$ is favorable whereas for high SFE steels ($>20 \text{ mJm}^{-2}$) the direct $\gamma \rightarrow \alpha'$ is often observed [3,5]. Twinning-Induced Plasticity (TWIP) in combination with TRIP occurs in higher SFE steels [6]. The general trend is that with increasing SFE the following sequence of predominant deformation mechanism is observed: TRIP $\gamma \rightarrow \varepsilon \rightarrow \alpha'$, TRIP $\gamma \rightarrow \alpha'$, TWIP and slip [3,5–7].

The amount of α' -martensite formed during straining has important implications on the formability during cold forming processes [8,9]. During forming, parts of the components are subjected to uniaxial strain paths or more complex loading states. How the loading state influences

the transformation characteristics has been addressed in a few studies but remains inconclusive. It has been reported for 304 steels that a biaxial tension enhances the martensitic transformation [10,11]. However other reports on 201, Fe18Cr10Ni (at low temperature) and 301LN steels show that uniaxial loading produces more martensite than biaxial loading [12–15]. The majority of the above mentioned studies were conducted on punched sheet samples where different locations exhibit different loading states, including uniaxial and equibiaxial tension. Microscopic observations have suggested that an increased density of dislocations under biaxial loading results in higher amount of martensite [13]. A detailed understanding of the role of the loading state is however missing.

Transformation kinetic models have helped in understanding the matter, but several points remain unclear. Some models suggest that a higher triaxiality factor Σ , i.e. the ratio of hydrostatic stress and the Von Mises stress, leads to a higher amount of formed martensite [16, 17]. Such models predict that when e.g. loading equibiaxially (i.e. $\Sigma = 0.67$) will result in a higher amount of martensite than when loading uniaxially (i.e. $\Sigma = 0.33$). On the other hand, a recent kinetic model suggests that the fraction of strain-induced martensite does not only depend on the triaxiality factor but also on the Lode angle parameter: if this is the case, uniaxial loading produces more martensite than equibiaxial, as is for example observed for 301LN steel [14]. The above-mentioned kinetic models consider solely the mechanics of plasticity and phase transformations, do not consider microstructural properties such as for instance the evolving crystallographic texture during

* Corresponding author.

E-mail address: helena.vs@psi.ch (H. Van Swygenhoven).

loading and cannot explain the dependence of the intermediate ε -martensite on the strain path.

In the present study we address the effect of loading state on the transformation behavior of a low SFE austenitic stainless steel exhibiting the $\gamma \rightarrow \varepsilon \rightarrow \alpha'$ transformation sequence. A commercial 201 stainless steel is employed having a mean grain size of $45 \mu\text{m}$ and a nominal composition of Fe-16-18Cr-5.5-7.5Mn-3.5-5.5Ni-max1Si-max0.15C (wt%), which according to the empirical relationships of Ref. [18,19] has a SFE $\sim 20 \pm 3 \text{ mJm}^{-2}$. Cruciform-shaped and dogbone samples were deformed (both uniaxially and cruciforms equibiaxially) during neutron diffraction allowing the observation of ε - and α' -martensite evolution. The cruciform geometry was optimized with the aid of FE analysis using ABAQUS, the employed geometry is shown in the supplementary material S1a.

In situ neutron diffraction tests were carried out at the POLDI beamline of the Swiss neutron spallation source SINQ which is equipped with a biaxial machine and a tensile machine [20,21]. A schematic of the experimental setup is shown in the supplementary material S1c. The in-plane strain was measured with a 2-camera digital image correlation (DIC) system (GOM, Aramis 5M). Uniaxial loading (hereafter referred as UN) and equibiaxial loading (hereafter referred as EQ) were performed with a loading rate of 80 N/s. The uniaxial loading direction F2 was parallel to the rolling direction, RD, of the sheet (see supplementary material S1b), the equibiaxial load was performed along RD and TD. A uniaxial test was performed on a dogbone-shaped specimen (see supplementary material S1b) and the results were consistent with the UN cruciform sample. Neutron diffraction measurements were carried out in predefined force intervals upon interrupting the loading and holding the displacement until the sample was fractured. The maximum

equivalent strain that could be reached during the equibiaxial test was $\sim 16\%$, a limitation caused by the stress concentrations at the cross-arms of the cruciform specimen. The maximum strain reached under uniaxial tension was 29%. The neutron diffraction data were analyzed with the open source software Mantid [22].

EBSID studies were carried out on the as-received and on the deformed material. For the latter, additional samples were deformed uniaxially (dogbone) and equibiaxially (cruciform) up to 13% equivalent strain in order to obtain samples at comparable strains. The samples were ground with 1200 grit SiC paper and then electropolished for 5 s with a 16:3:1 (by volume) methanol, glycerol and perchloric acid solution. A field emission gun scanning electron microscope (FEG SEM) Zeiss ULTRA 55 equipped with EDAX Hikari Camera operated at 20 kV in high current mode with $120 \mu\text{m}$ aperture was used. The EBSD raw data were post-processed using the EDAX OIM Analysis 7.3 software.

The evolution of the neutron diffraction patterns during deformation is shown in Fig. 1a and b for the UN and EQ samples respectively. Initially only austenite reflections are observed. After $\sim 10\%$ strain (which corresponds to a true stress value of $\sim 645 \text{ MPa}$, obtained from the dogbone sample) a reflection corresponding to $(10\bar{1}1)_\varepsilon$ ε -martensite appears in the UN sample. The $110_{\alpha'}$ α' -martensite reflection appears only after 23% strain, which corresponds to a true stress value of $\sim 1000 \text{ MPa}$, obtained from the dogbone sample. The increase in the α' intensity is accompanied by a decrease in the intensity of ε , as can be observed in Fig. 1c where both reflections are compared at 20% and 29% strain. On the other hand, no reflections corresponding to ε - or α' -martensite are observed for the EQ sample up to 16% equivalent strain. A comparison of the neutron diffraction patterns at $\sim 16\%$ equivalent strain is given

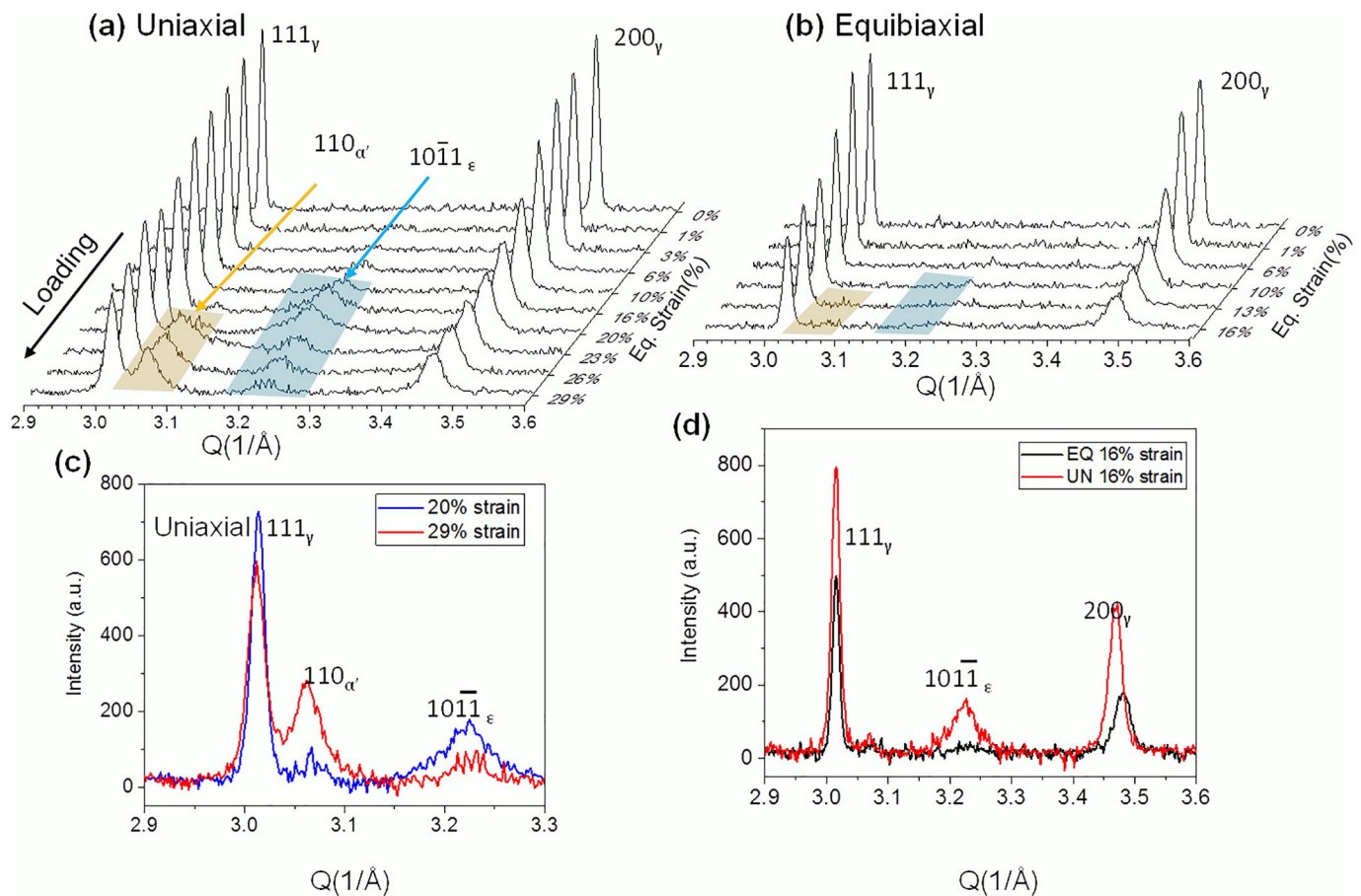


Fig. 1. Neutron diffraction patterns with increasing the applied strain for (a) uniaxial loading and (b) equibiaxial loading. (c) Comparison of the diffraction patterns at 20% and 29% equivalent strain for the UN sample, showing the increase of α' -martensite fraction in expense of ε -martensite. (d) Comparison of the diffraction patterns from the UN and EQ samples at 16% equivalent strain.

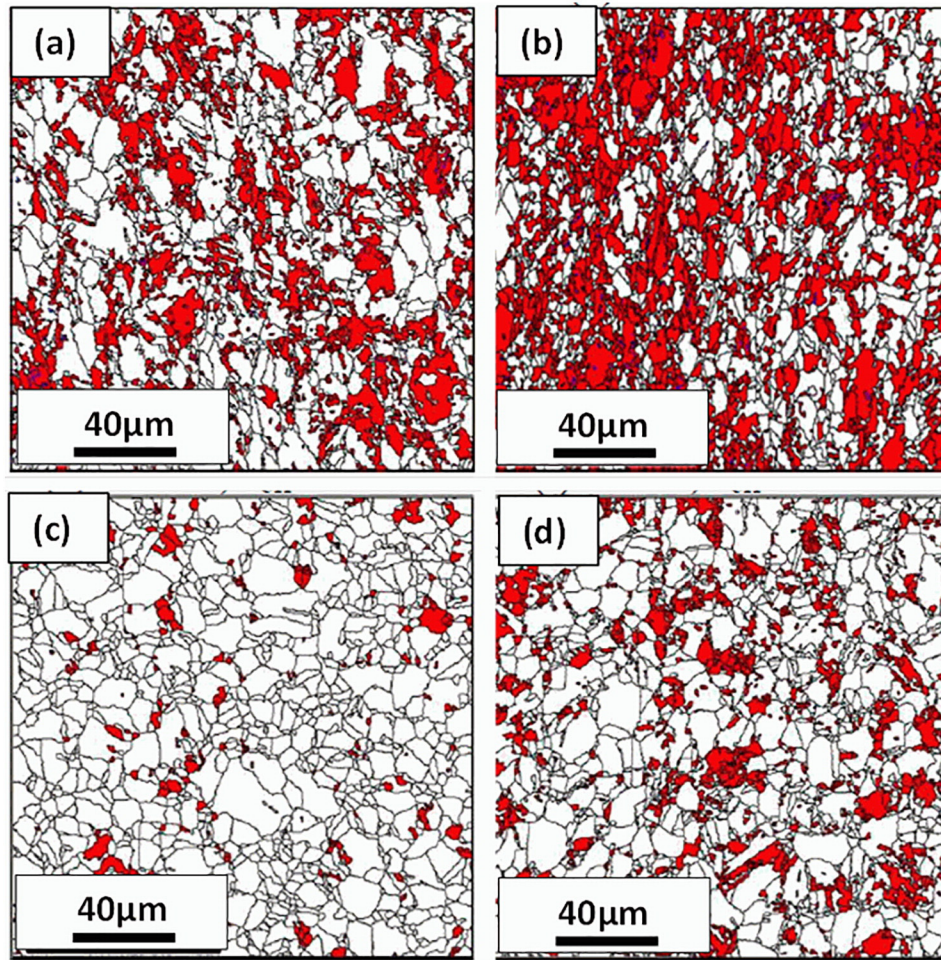


Fig. 2. Phase maps showing γ -austenite (white) and α' -martensite (red) after: uniaxial tension at a) 21% and b) 35% and biaxial tension at c) 22%, d) 34% equivalent strain [15].

in Fig. 1d, showing the absence of any martensite reflection in the EQ sample, as opposed to the UN sample having a pronounced $10\bar{1}1_g$ reflection. To verify whether transformation occurs under equibiaxial loading, a sample was deformed by a hemispherical punch allowing reaching much larger biaxial strains than the in-situ tests [15]. Fig. 2 shows the phase maps from EBSD analysis taken from areas deformed up to 21% and 35% uniaxial strain and from areas deformed to 22% and 34% equivalent biaxial strain. These observations confirm that the formation of α' -martensite occurs also under biaxial loading state, however, the transformation is significantly less abundant than the uniaxial loading.

The question arises why the martensitic transformation is suppressed during equibiaxial loading. To understand this, the mechanism of ε -martensite formation needs to be considered. According to the theory of Olson and Cohen [23], the deformation-induced hexagonal domains are formed by the arrangement of stacking faults, resulting from the dissociation of perfect dislocations, into two partials on every second $\{111\}$ plane. The separation between the Leading Partial Dislocations (LPDs) and the Trailing Partial Dislocations (TPDs) can be altered by local or external applied stresses: a typical equilibrium separation of ~ 10 nm can increase up to $\sim 1 \mu\text{m}$ [24]. This is for instance the case when the LPD has a higher Schmid factor than the TPD: the large separation between the partials results then in the local appearance of the hexagonal ε -martensite phase [24,25]. In the opposite case, when the TPD has a higher Schmid factor, the system becomes unfavorable to the formation of ε -martensite and hence conventional dislocation slip occurs. During uniaxial and equibiaxial loading, different deformation

textures are formed which in turn would influence the Schmid factors of the partial dislocations under the different loading conditions. The Schmid factors of the partial dislocations corresponding to the slip system with the highest Schmid factor were calculated under uniaxial loading along RD and in-plane equibiaxial loading for the $\langle 111 \rangle$, $\langle 001 \rangle$, $\langle 101 \rangle$, $\langle 102 \rangle$ and $\langle 113 \rangle$ orientations (see supplementary material, S2 and S3). For the equibiaxial case it should be noted that for the Schmid factor calculation, the in-plane equibiaxial loading is equivalent to uniaxial compression along the normal direction (ND). Moreover, in the case of compressive loading the situation is reversed since changing the direction of the applied stress changes the sense of glide motion of the partial dislocations, such that the LPD becomes TPD and vice versa [26]. The inverse pole figures (IPFs) for RD, TD and ND of the 201 material before deformation (3a) and after uniaxial (3b) and biaxial deformation (3c), both at 13% equivalent strain are shown in Fig. 3. For uniaxial deformation along RD (Fig. 3b for the IPF along RD) the LPDs have a higher Schmid factor on the right hand side of the boundary, as indicated by area enclosed by the dashed line. For these grains, the formation of ε -martensite is possible. For grains with orientations on the left side of the boundary, the LPDs have lower Schmid factor than the TPDs and therefore ε -martensite is not likely to form. For equibiaxial deformation the grains which facilitate the formation of ε -martensite are contained in the dashed area on the left hand side of the $\langle 113 \rangle$ - $\langle 102 \rangle$ boundary as shown in Fig. 3c for the IPF along ND. In both cases, the closer to the $\langle 113 \rangle$ - $\langle 102 \rangle$ boundary an orientation is, the smallest the difference of the Schmid factors between the two partial dislocations is.

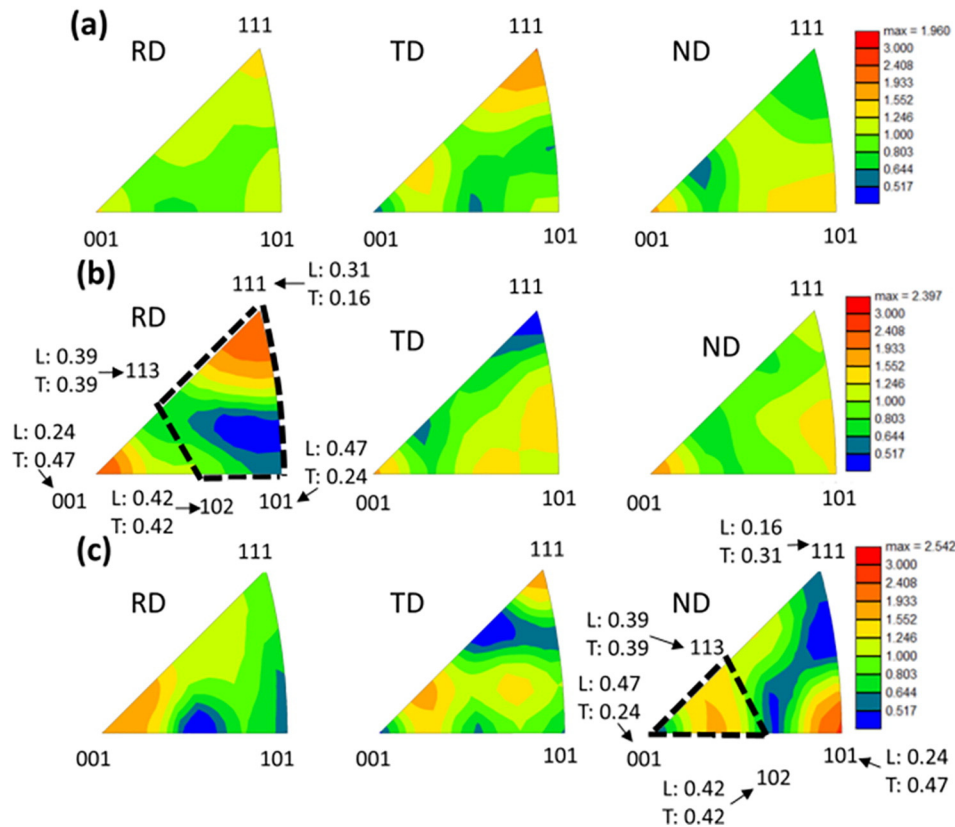


Fig. 3. IPFs of the (a) as-received (b) uniaxially-deformed (along RD) up to ~13% strain and (c) equibiaxially-deformed (along RD and TD) up to ~13% equivalent strain 201 SS material along the three principal sample directions. Note the highlighted IPFs in (b) and (c), they correspond to (b) uniaxial loading along RD and (c) equibiaxial (along RD and TD) or uniaxial compression along (ND). The enclosed regions, with dashed lines, indicate the orientations for which the LPDs have higher Schmid factor than the TPDs. The Schmid factor values for the leading and trailing partial dislocations (denoted with L and T respectively) are also given.

The above results indicate that the deformation textures formed during uniaxial and equibiaxial loading play a significant role on the appearance/absence of ε -martensite. The as-received material exhibits only a very mild texture as shown in the IPFs of Fig. 3a. However, as shown in the IPF maps along RD, TD and ND shown in Fig. 3b and c, the texture formed after 13% strain during uniaxial and equibiaxial deformation is already different. In the uniaxial deformed sample a bimodal texture exhibiting a strong $\langle 111 \rangle$ and a less pronounced $\langle 001 \rangle$ pole parallel to the RD direction (also the loading direction) is obtained. The strongest pole in the UN sample is lying in the area for which the LPDs have higher Schmid factor than the TPDs. In contrast, under equibiaxial loading, a $\langle 110 \rangle$ texture forms parallel to the ND direction: the strongest pole belongs to that part of the IPF where the TPDs have higher Schmid factor than the LPDs and these grain orientations are not favorable for the formation of ε -martensite. Quantitatively, by integrating the IPFs, weighted by grain area, it is obtained that ~81% of the scanned area favors the formation of ε -martensite in the uniaxial loading case, whereas only ~49% in the equibiaxial loading case.

Fig. 4 illustrates parts of these areas where these differences are shown in a more detailed microstructural view after 13% strain. In these figures, the grains that belong to the orientations for which the LPDs have a higher Schmid factor are colored blue, the grains for which the TPDs have a higher Schmid factor are red, ε -martensite is green and α' -martensite is yellow. After uniaxial deformation (Fig. 4a and c) the majority of the grains are blue and most of them contain significant amounts of martensite. After equibiaxial deformation (Fig. 4b and d) there are less blue grains with little martensite. Interestingly, the blue grains in the EQ sample contain very little ε -martensite compared to the blue grains in the UN sample. To understand this, the

orientation of the grains containing most martensite which are the blue grains A-D in the UN sample and the blue grains E-H in the EQ sample are shown in Fig. 4e and f. In the UN sample the orientation of grains A-D lies close to the $\langle 111 \rangle$ orientation for which the difference between the Schmid factor of the LPDs and the TPDs is the highest (see Fig. 4e). In contrast, the grains that exhibit transformation under equibiaxial loading have orientations close to the “neutral” $\langle 113 \rangle$ - $\langle 102 \rangle$ boundary (see grains E, F, and G in Fig. 4f). Because the difference between the Schmid factor of LPDs and TPDs is not very high, the transformation here is limited. This is confirmed by the absence of visible martensite in grain D in the UN sample and grain H in the EQ sample, both having their orientation close to the “neutral” $\langle 113 \rangle$ - $\langle 102 \rangle$ line. Furthermore it can be noted that, since α' -martensite appears at the intersections of the ε -martensite bands in the EQ sample, the EBSD measurements confirm that ε -martensite is a precursor for α' -martensite during uniaxial and equibiaxial deformation, as was also demonstrated in the neutron diffraction results for uniaxial deformation. The fact that ε -martensite is not observed by the neutron measurement, during equibiaxial deformation, has to be ascribed to a combination of the suppression of formation, the limited equivalent strain reached with the cruciform geometry and the detection limit of the method.

In summary, in-situ neutron diffraction studies performed on metastable 201 stainless steel combined with EBSD measurements confirm that ε -martensite is a precursor for α' -martensite during uniaxial and equibiaxial deformation at the same loading rate. In both loading states, the grains that contain martensite belong to orientations for which the LPDs have higher Schmid factor than the TPDs. The martensitic transformation is suppressed during equibiaxial loading as a consequence of the different textures formed during deformation.

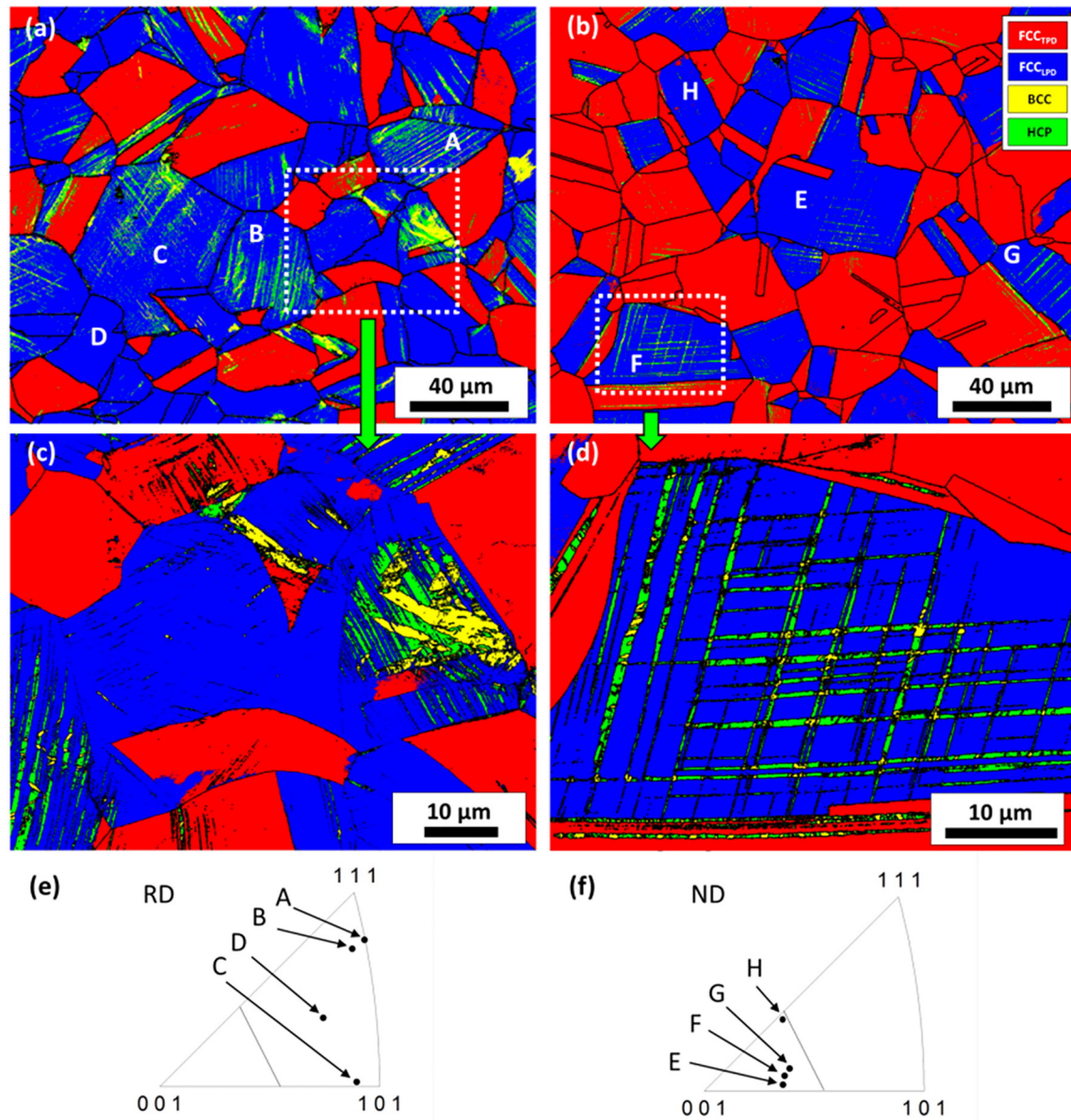


Fig. 4. Phase maps showing the γ -austenite grains which belong to the “high Schmid factor” orientation regime for the LPDs (with blue) and the “high Schmid factor” orientation regime for the TPDs (with red), ε -martensite and α' -martensite for: (a) uniaxial, (b) equibiaxial both at $\sim 13\%$ equivalent strain. (c) Magnification of the highlighted area in (a) showing significant amount of α' -martensite within the bands of ε -martensite. (d) Magnification of the highlighted area in (b) showing that α' -martensite forms at the intersection of ε -martensite. The indicated grains A–H and their corresponding position in the IPF are shown in (e) for uniaxial tension and (f) for equibiaxial tension.

Acknowledgements

E.P., W.-N.H., M.S. and H.V.S. thank the European Research Council for the financial support within the ERC-advanced grant MULTIAx (339245). E.P. acknowledges Dr. S. Martin (with TU Freiberg) for the helpful discussion on the matter.

Appendix A. Supplementary data

Supplementary data to this article can be found online at <https://doi.org/10.1016/j.scriptamat.2017.12.026>.

References

- [1] R.P. Reed, *Acta Metall.* 10 (1962) 865–877.
- [2] G.B. Olson, M. Cohen, *Metall. Trans. A* 6 (1975) 791–795.
- [3] P. Behjati, A. Najafizadeh, *Metall. Trans. A* 42 (2011) 3752–3760.
- [4] M.C. McGrath, D.C. Van Aken, N.I. Medvedeva, J.E. Medvedeva, *Metall. Trans. A* 44 (2013) 4634–4643.
- [5] K. Sato, M. Ichinose, Y. Hirotsu, Y. Inoue, *ISIJ Int.* 29 (1989) 868–877.
- [6] T.-H. Lee, E. Shin, C.-S. Oh, H.-Y. Ha, S.-J. Kim, *Acta Mater.* 58 (2010) 3173–3186.
- [7] J.E. Wittig, M. Pozuelo, J.A. Jiménez, G. Frommeyer, *Steel Res. Int.* 80 (2009) 66–70.
- [8] S. Papula, J. Talonen, H. Hänninen, *Metall. Trans. A* 45 (2014) 1238–1246.
- [9] V. Talyan, R.H. Wagoner, J.K. Lee, *Metall. Trans. A* 29 (1998) 2161–2172.
- [10] S.S. Hecker, M.G. Stout, K.P. Staudhammer, J.L. Smith, *Metall. Trans. A* 13 (1982) 619–626.
- [11] L.E. Murr, K.P. Staudhammer, S.S. Hecker, *Metall. Trans. A* 13 (1982) 627–635.
- [12] A.A. Lebedev, V.V. Kosarchuk, *Int. J. Plast.* 16 (2000) 749–767.
- [13] S.B. Nizhnik, B.I. Koval'chuk, É.S. Istomina, E.A. Dmitrieva, *Strength Mater.* 10 (1978) 77–83.
- [14] A.M. Beese, D. Mohr, *Acta Mater.* 59 (2011) 2589–2600.
- [15] S. Chakrabarty, PhD Thesis, IIT Bombay, Mumbai India, 2015.
- [16] G.N. Haidemenopoulos, N. Aravas, I. Bellas, *Mater. Sci. Eng. A* 615 (2014) 416–423.
- [17] R.G. Stringfellow, D.M. Parks, G.B. Olson, *Acta Metall. Mater.* 40 (1992) 1703.
- [18] P.J. Brofman, G.S. Ansell, *Metall. Trans. A* 9 (1978) 879–880.
- [19] M. Moallemi, A. Kermanpur, A. Najafizadeh, A. Rezaee, H.S. Baghbadorani, P.D. Nezhadfar, *Mater. Sci. Eng. A* 653 (2016) 147–152.

- [20] S. Van Petegem, J. Wagner, T. Panzner, M.V. Upadhyay, T.T.T. Trang, H. Van Swygenhoven, *Acta Mater.* 105 (2016) 404–416.
- [21] U. Stuhr, M. Grosse, W. Wagner, *Mater. Sci. Eng. A* 437 (2006) 134–138.
- [22] O. Arnold, J.C. Bilheux, J.M. Borreguero, A. Buts, S.I. Campbell, L. Chapon, M. Doucet, N. Draper, R. Ferraz Leal, M.A. Gigg, V.E. Lynch, A. Markvardsen, D.J. Mikkelsen, R.L. Mikkelsen, R. Miller, K. Palmen, P. Parker, G. Passos, T.G. Perring, P.F. Peterson, S. Ren, M.A. Reuter, A.T. Savici, J.W. Taylor, R.J. Taylor, R. Tolchenov, W. Zhou, J. Zikovsky, *Nucl. Inst. Methods Phys. Res. A* 764 (2014) 156–166.
- [23] G.B. Olson, M. Cohen, *Metall. Trans. A* 7 (1976) 1897–1904.
- [24] T.S. Byun, *Acta Mater.* 51 (2003) 3063–3071.
- [25] S. Martin, C. Ullrich, D. Rafaja, *Mater. Today: Proc.* 2 (2015) S643–S646.
- [26] S.M. Copley, B.H. Kear, *Acta Metall.* 16 (1968) 227–231.